

Theoretical investigation of the interaction between the metal phthalocyanine [MPc]^a (M = Sc, Ti, and V; a = -1, 0, and +1) complexes and formaldehyde

Nasim HASSANI* 

Department of Chemistry, College of Sciences, Shiraz University, Shiraz, Iran

Received: 03.06.2020 • Accepted/Published Online: 23.10.2020 • Final Version: 17.02.2021

Abstract: Formaldehyde (FA, CH₂O) is one of the toxic volatile organic compounds that cause harmful effects on the human body. In this work, the interaction of FA gas with metal phthalocyanine (MPc) molecules was studied by employing density functional theory calculations. A variety of [MPc]^a (M = Sc, Ti, and V; a = -1, 0, and +1) complexes were studied, and the electronic properties, interaction energies, and charge transfer properties of all of the studied molecules were systematically discussed. Among the studied complexes, the Sc and Ti phthalocyanines were more reactive toward the adsorption of FA gas. Moreover, it was revealed that the interaction of the [ScPc]⁺¹ and [TiPc]⁰ complexes with the CH₂O molecule was stronger, in which the highest occupied molecular orbital (HOMO) and lowest unoccupied molecular orbital (LUMO) energy gap of 46% and 36% decreased after FA adsorption. The results indicated that the MPc-based materials may be a promising candidate for the detection of FA gas.

Key words: Metal phthalocyanine, formaldehyde, electronic properties, HOMO-LUMO energy gap, gas detection, DFT

1. Introduction

Formaldehyde (FA, CH₂O) is a toxic gas that is exposed to indoor air through manufacturing processes [1,2]. Increasing the concentration of FA in the air leads to adverse health effects on humans and animals. Consequently, to accurately control the concentration of FA in ambient air, it is urgent that new sensing material for detection of the FA is developed.

During recent last decades, various materials have demonstrated the potential to become a chemical sensor, such as carbon nanotube [3], the nanowire of various materials [4–8], nanoparticle arrays [9], mono-layer capped metal nanoparticles [10], metal oxides [11]. Sensors based on metal phthalocyanines (MPcs) are one of the best materials available to detect gases, because they offer a small-size, high-sensitivity, low-cost, ease of synthesis, and low processing temperature [12–14]. In addition, MPc aromatic macrocycles have the ability to stack and form crystalline and poly-crystalline films, which make these molecules appropriate for the design of field-effect transistors [15,16]. Furthermore, MPc-based sensors have shown strong absorption in ultraviolet-visible and near-infrared regions, which is why these molecules are used for photodynamic therapy for cancer [17,18].

Several studies based on MPc have been conducted in chemical sensing. The results revealed that by varying the central metal ions of the MPc, the ionization potential, optical properties, sensitivity, and selectivity could change when in contact with different gas molecules. For example, Rossignol et al. [19] studied the detection of the NH₃ and O₃ gases in the range of 20 to 200 ppm using a cobalt phthalocyanine sensor. Moreover, there has been a lot of research conducted on the detection of NO₂ and NH₃ with MPcs (M = Pd, Co, Cu, Mg, Ti, Ni, and Zn) [20–24]. It is important to mention that a well-known phthalocyanine complex of titanium and vanadium is the metal-oxo complex, with a M⁴⁺ redox state (M = Ti and V) [25,26]. However, under some particular chemical conditions, low-valent metal species could be stable. For example, Eguchi et al. [27], in their experimental investigation, synthesized the VPc monolayer on the Ag (111) under ultra-high-vacuum condition. The variation of the axial ligands, the functional groups of the side chains, and μ -bridging atom is able to induce different electronic properties to the MPc complexes. Consequently, by designing and optimizing these synthesized thin films, it is possible to produce MPcs with different degrees of sensitivity, selectivity, and stability. In this regard, Blowey et al. [28], in their valuable study, demonstrated that vanadyl phthalocyanine (VOPc) can stabilize on the surface of Cu (111) from the up and down orientations of the V = O moiety. Moreover, the surface of the VPc complex (VOPc without axial oxygen) was actually available in the down orientation of the VOPc complex. Lu et al. [29] conducted

* Correspondence: nasim.hassani.chem@gmail.com

a systematic study of the ability of the porous sheet of MPc (Sc to Zn) toward hydrogen storage. They concluded that the ScPc sheet was able to store 4.6% hydrogen and might be a promising material for H₂ storage. However, there are a few studies on the application of MPc complexes (M = Sc, Ti, and V).

The ability of transition MPc in the interaction with different gases, on one side, and the existence of the CH₂O molecule in ambient air as a pollutant, on the other side, provided the motivated herein to study the interaction of MPc (M = Sc, Ti, and V) complexes with FA gas. Arokianathan et al. [30] showed that the substitution of functional groups did not affect the properties of the MPc ring (Sc and Mg). Accordingly, to reduce the computational cost, the effect of the axial groups, functional groups, and substrates that were present in many synthesized MPc complexes were not considered herein. All in all, in the current work, the electronic properties and adsorption behaviors of the [MPc]^a (M = Sc, Ti, and V; a = -1, 0, 1) complexes toward the FA molecule were studied. The interaction of H₂CO with the three considered forms of the [MPc]^a (-1, 0, and +1) complexes was investigated based on analyses of the preferable orientations, electronic properties, and corresponding binding energies within the density functional theory (DFT) framework.

2. Computational details

All of the calculations performed herein were conducted using the Kohn-Sham DFT with the Becke three-parameter hybrid, non-local exchange, and correlation functional, known as B3LYP [31,32], in conjunction with the split-valence basis set 6-31G* for the H, N, C, and O atoms, and the LANL2DZ basis set for the transition metals, as implemented in the Gaussian 09 program (Gaussian, Inc., Wallingford, CT, USA) [33]. Moreover, previous studies revealed that the use of the B3LYP functional performs reasonably well to predict ground-state properties and gas adsorption on the MPc complexes [34–38]. The validity of the global minimum was determined using the calculation of the vibrational frequencies, in which the absence of vibrational modes with imaginary frequencies demonstrated that the optimized molecular geometry was found at the lowest energy structure. The values of the atomic charges were estimated by employing natural bond orbital (NBO) analysis with the same geometry optimization level. In addition, to obtain accurate results for adsorption of the gases over the MPcs, and taking into account the Van der Waals forces, the results were obtained by considering the long-range correction scheme introduced by Grimme (i.e. the D3-DFT method) [39].

The zero-point energy (ZPE) corrected interaction energy (E_{int}) for the complexes were calculated by employing the following formula:

$$E_{int} = (E_{Gas-PMc} - E_{PMc} - E_{Gas}) + (E_{Gas-PMc}^{ZPE} - E_{PMc}^{ZPE} - E_{Gas}^{ZPE}) + BSSE \quad (1)$$

Here, $E_{Gas-PMc}$ is the total energy of [Gas/MPc] complex, and E_{PMc} and E_{Gas} are the calculated energies for the pure MPc complex and the gas molecule, respectively. Based on the obtained results, a negative value of E_{int} showed that the adsorption process had an exothermic character. Furthermore, the basis set superposition error was eliminated by taking into account the standard counterpoise correction method of Boys and Bernardi [40].

the highest occupied molecular orbital (HOMO) and lowest unoccupied molecular orbital (LUMO) energy gap (HOMO–LUMO) (E_g) was obtained using the following equation:

$$E_g = \epsilon_{LUMO} - \epsilon_{HOMO} \quad (2)$$

where ϵ_{LUMO} and ϵ_{HOMO} are the corresponding energies of the LUMO and HOMO, respectively.

The change in the HOMO-LUMO energy gap (ΔE_g) was calculated as in Eq. (3) for the [MPc]^a (M = Sc, Ti, and V; a = -1, 0, and +1) complexes toward the FA adsorption.

$$\Delta E_g = |(E_{g2} - E_{g1})/E_{g1}| \times 100 \quad (3)$$

Here, E_{g1} and E_{g2} are the values of E_g in the initial (bare [MPc]^a) and final state ([gas/MPcs]^a complexes), respectively.

3. Results

3.1. Electronic structure of the [ScPc]^a (a = -1, 0, and +1) complexes

The optimized structures of the [ScPc]^a (a = -1, 0, and +1) complexes are shown in Figure 1a. The data analyses showed that the ScPc in all three of the oxidized, neutral, and reduced states had a nonplanar geometric structure with C_{2v} symmetry. Moreover, the Sc atom was projected by about 1.115, 1.002, and 0.774 Å out of the molecular planes of the [ScPc]⁺¹, [ScPc]⁰, and [ScPc]⁻¹ complexes, respectively. It was found that increasing the negative charge on the ScPc complex reduced the out-of-plane projection of the Sc atom. The calculated Sc-N bond lengths were 2.086, 2.080, and 2.082 Å for the [ScPc]⁺¹, [ScPc]⁰, and [ScPc]⁻¹ complexes, respectively. These data also showed an increase of 0.006 and 0.002 Å in the Sc-N bond length in the oxidized and reduced states, which showed that these bonds were weaker than that of neutral state. Moreover,

the calculated bond orders for the Sc-N bond were 0.73 and 0.45 for the $[\text{ScPc}]^{-1}$ and $[\text{ScPc}]^0$ states, respectively, which demonstrated that this bond order decreased by inducing the positive charge on the ScPc complexes. Furthermore, increasing the positive charge on the ScPcs prevented the bond between the Sc and N atoms. In this regard, $[\text{ScPc}]^{+1}$ may be an unstable and more reactive complex.

Metal coordination is an important feature of the MPcs toward gas adsorption. In these structures the positively-charged M atoms coordinated to the four isoindole nitrogens of the phthalocyanine ring through covalent and electrostatic interactions. According to the NBO population analysis (see Table 1), the Sc atom presented a positive charge, with values of 1.89, 1.81, and 1.75 e for the $[\text{ScPc}]^{+1}$, $[\text{ScPc}]^0$, and $[\text{ScPc}]^{-1}$ complexes, respectively. The values of the charge on the Sc atom revealed that, when the ScPc complex was reduced, a part of the induced charge remained close to the Sc atom.

Frontier molecular orbitals (FMOs) are important descriptors used to better understand the stability and reactivity of the complexes. In the electrophilic attack, the ionization potential was related to the HOMO. In the nucleophilic reactions, electronic affinity, and susceptibility were directly related to the LUMO. Moreover, the HOMO–LUMO energy gap (E_g) can be utilized to estimate the chemical stability and reactivity of the complexes. The spatial distribution of the FMOs of the ScPcs are presented in Figure 1b, where it can be seen that the electron density of the HOMO and LUMO orbitals was uniformly distributed over the surfaces of the $[\text{ScPc}]^{-1}$ and $[\text{ScPc}]^0$ complexes. However, the HOMO of the $[\text{ScPc}]^{+1}$ complex was mainly localized on the phthalocyanine ring, without any contribution by the Sc atom. The E_g values of the $[\text{ScPc}]^{+1}$, $[\text{ScPc}]^0$, and $[\text{ScPc}]^{-1}$ complexes were 1.82, 1.18, and 1.26 eV, respectively. Therefore, as a result of the narrow HOMO-LUMO gap, the $[\text{ScPc}]^0$ complex was more reactive than its counterparts toward FA adsorption.

A map of electrostatic potential (MEP) is a physical descriptor to predict the active site of complexes upon nucleophilic and electrophilic attacks, where the positive and negative electrostatic potential regions are represented by the suitable part of a complex in electrophilic and nucleophilic attacks, respectively. The MEP of the ScPcs is shown in Figure 1c, which demonstrates the distribution of negative and positive electrostatic potential regions on the ScPcs. Moreover, in all of the complexes, the positive region (in blue) is mainly localized on the Sc atom. Thus, the Sc atom had more potential to participate in the nucleophilic attack.

3.2. Electronic structure of the $[\text{TiPc}]^a$ ($a = -1, 0, \text{ and } +1$) complexes

The optimized structures of the $[\text{TiPc}]^a$ ($a = -1, 0, \text{ and } +1$) complexes are shown in Figure 2a. Although both the $[\text{TiPc}]^{-1}$ and $[\text{TiPc}]^0$ complexes were completely planar, the $[\text{TiPc}]^{+1}$ complex had a nonplanar structure, in which the Ti atom was about 0.814 Å out of the molecular plane. The calculated Ti-N bond distances were 2.012, 2.015, and 2.009 Å for the $[\text{TiPc}]^{+1}$, $[\text{TiPc}]^0$, and $[\text{TiPc}]^{-1}$ complexes, respectively. These results showed that the Ti-N bond lengths in the reduced and oxidized states were 0.006 and 0.003 Å less than in the neutral state, which showed that this bond was stronger than that of their neutral counterparts.

The NBO analysis revealed that there was no actual bond between the Ti and N atoms in any of the three considered TiPc complexes, which explained why the isolated TiPc complex was not observed experimentally. Accordingly, to stabilize the TiPc complexes, it is important to use a substrate. However, the oxo-TiPc adsorbed from the O-head on a substrate or the directly synthesized TiPc on a surface may be used as a bare TiPc complex in practical applications. The base on the NBO analysis (see Table 1) and the titanium atoms present positive charges, at values of 1.42, 1.37, and 1.15 e in the $[\text{TiPc}]^{+1}$, $[\text{TiPc}]^0$, and $[\text{TiPc}]^{-1}$ complexes, respectively, were due to the fact that a part of the induced charge remained close to the Ti atom after reducing the TiPc complex.

According to the spatial distribution of the FMOs of TiPc complexes (see Figure 2b), the LUMOs of $[\text{TiPc}]^{-1}$ and $[\text{TiPc}]^0$ complexes were more localized on the Ti atom, which indicated that when these complexes were attacked by a nucleophilic compound, the electrons went to the d orbital of the Ti atom. This was further confirmed by the MEP plots, where the positive charges were distributed across the Ti atom and created an electric field on the surface of the $[\text{TiPc}]^{-1}$ and $[\text{TiPc}]^0$ complexes (see Figure 2c). This may lead to the polarization of the incoming gas molecules during nucleophilic attacks.

The E_g values of the $[\text{TiPc}]^{+1}$, $[\text{TiPc}]^0$, and $[\text{TiPc}]^{-1}$ complexes were 1.58, 2.37, and 2.20 eV, respectively. Accordingly, the reactivity of the TiPc complexes toward gas adsorption decreased in the order of $[\text{TiPc}]^{+1} > [\text{TiPc}]^{-1} > [\text{TiPc}]^0$.

3.3. Electronic structure of the $[\text{VPc}]^a$ ($a = -1, 0, \text{ and } +1$) complexes

The optimized $[\text{VPc}]^{-1}$ and $[\text{VPc}]^0$ complexes were completely planar (see Figure 3a), while the structure of the $[\text{VPc}]^{+1}$ complex had a curvature, and one of its sides was about 1.001 Å higher than the other side. The calculated V-N bond lengths were 2.009, 1.999, and 1.996 Å in the $[\text{VPc}]^{+1}$, $[\text{VPc}]^0$, and $[\text{VPc}]^{-1}$ complexes, respectively. These results showed that the V-N bond lengths in the oxidized and neutral states were 0.010 and 0.013 Å higher than in the reduced state, which showed that this bond was weaker than that of their reduced counterparts.

The NBO population analysis (see Table 1) showed that the vanadium atom presented a positive charge, with values of 1.06, 0.96, and 0.82 e in the $[\text{VPc}]^{+1}$, $[\text{VPc}]^0$, and $[\text{VPc}]^{-1}$ complexes, respectively. Clearly, the charge in the V atom was

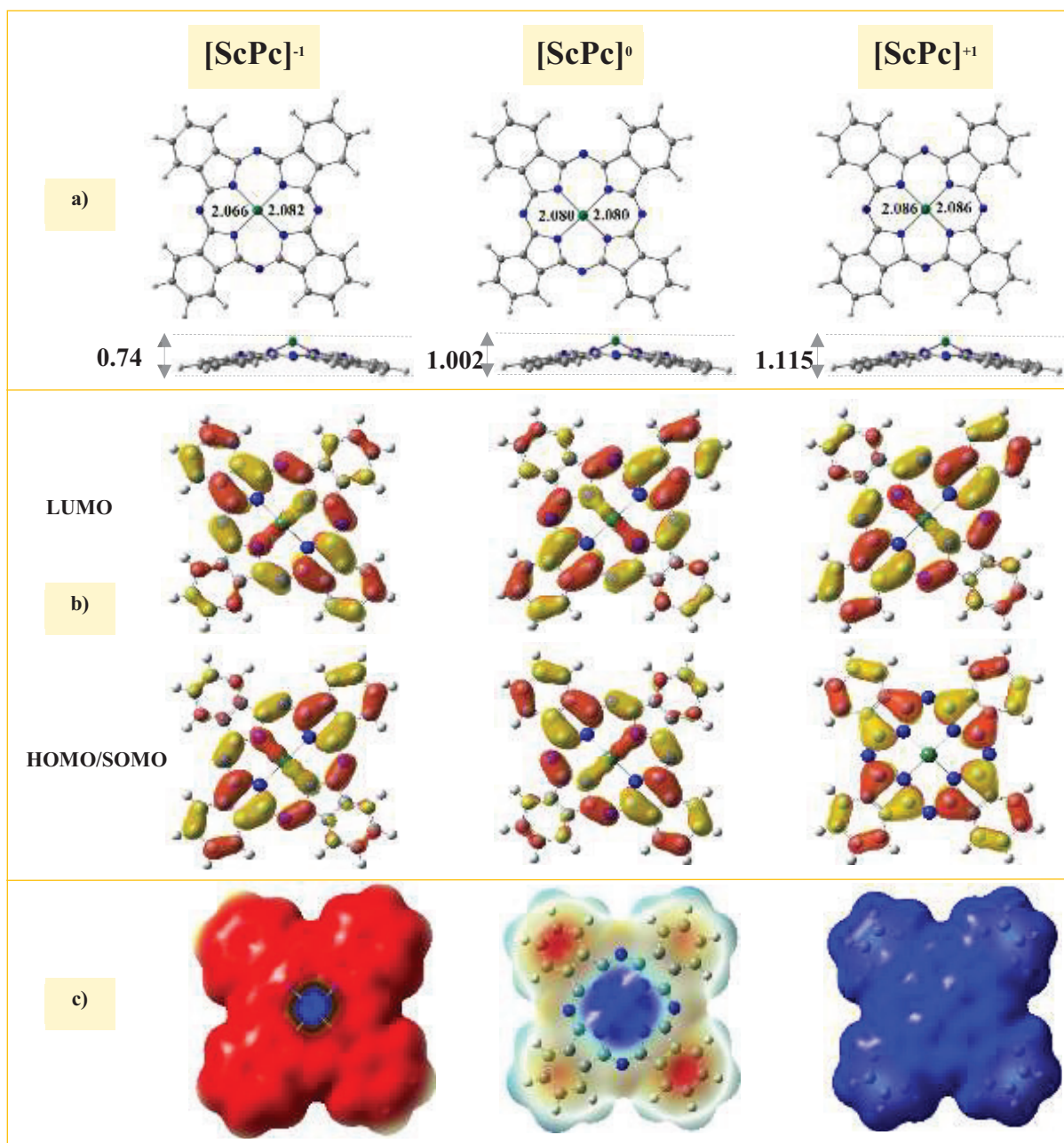


Figure 1. Calculated properties of the $[\text{ScPc}]^a$ ($a = -1, 0, \text{ and } +1$) complexes. a) Top and side views of the optimized structures with the bond distances in Å, b) SOMO/HOMO and LUMO spatial distributions with an isovalue of $0.02 \text{ e}/\text{Å}^3$, and c) molecular electrostatic potential isosurface (0.0004 au). The C, H, N, and Sc atoms are shown in grey, white, blue, and green, respectively.

more altered with the induction of both the positive and negative charges, in which a part of the induced charge remained close to the V atom.

Based on the spatial distribution of the FMOs (see Figure 3b), it was observed that the LUMOs of the $[\text{VPc}]^0$ and $[\text{VPc}]^{+1}$ complexes protruded more from the molecular plane, which indicated that the V atom of these complexes can be used as a target site under nucleophilic attacks. In the case of the $[\text{VPc}]^{-1}$ complex, the HOMO was mainly localized on the V atom, which demonstrated that when an electron was extracted from this complex, the extracted electron was from the V atom. The negative electrostatic potential was mainly localized on the whole surface of the $[\text{VPc}]^{-1}$ complex, which suggested that the $[\text{VPc}]^{-1}$ complex may be inert under nucleophilic attacks (see Figure 3c). The E_g values of the $[\text{VPc}]^{+1}$,

Table 1. Spin multiplicity ($2S+1$), SOMO¹/HOMO energy ($E_{SOMO/HOMO}$, in eV), LUMO energy (E_{LUMO} , in eV), SOMO-LUMO energy gap (E_g , in eV), and NBO charge on the M atom (q_M) for the bare [MPc]^a (M = Sc, Ti, and V; a = -1, 0, and +1) complexes.

[MPc]	2S+1	E_g	$E_{SOMO/HOMO}$	E_{LUMO}	q_M
[ScPc] ⁻¹	1	1.26	-0.96*	0.30	1.75
[ScPc] ⁰	2	1.18	-4.03	-2.85	1.81
[ScPc] ⁺¹	1	1.82	-7.86*	-6.04	1.89
[TiPc] ⁻¹	4	2.20	-1.13	1.07	1.15
[TiPc] ⁰	3	2.37	-4.79	-2.42	1.37
[TiPc] ⁺¹	2	1.58	-7.97	-6.39	1.42
[VPc] ⁻¹	5	2.17	-1.23	0.94	0.82
[VPc] ⁰	2	2.34	-5.13	-2.79	0.96
[VPc] ⁺¹	3	1.19	-8.32	-7.12	1.06

* Values with asterisks are related to the energy of HOMO.

¹ SOMO: singly-occupied molecular orbital.

[VPc]⁰, and [VPc]⁻¹ complexes were 1.19, 2.34, and 2.17 eV, respectively. It was predicted that the [VPc]⁺¹ complex may be more reactive than its counterparts towards gas adsorption.

3.4. Formaldehyde adsorption on the metal phthalocyanine complexes ([MPc]^a, M = Sc, Ti, and V; a = -1, 0, and +1)

Based on the results, the calculated C-H bond length and H-C-H bond angle of the free CH₂O was 1.11 Å and 115.2°, which was in good agreement with the reported experimental data of 1.01 Å and 118°, respectively [41]. These results suggested that the theoretical method used in this study was accurate to describe the studied system.

In order to obtain the stable structure of the CH₂O adsorbed on the surface of the MPcs, several possible initial adsorption geometries were considered, including the hydrogen site, oxygen site, and CH₂O surface perpendicular or parallel to the surface of the MPcs. However, the adsorption of the CH₂O from the O-side led to a more stable structure that was in good accordance with other theoretical and experimental studies [42–44].

Figure 4 shows the calculation results, where it can be seen that the Sc-O bond lengths in the reduced and oxidized states were 0.002 and 0.241 Å less than that of the neutral state. It was obvious that the [ScPc]⁺¹ complex had less tendency to adsorb the FA gas in comparison with the other studied Sc complexes. Moreover, the projection of the Sc atom from the plane of the [CH₂O/ScPc]^a complex was ~0.17 Å smaller than that of the bare clusters. This clearly demonstrated that the adsorption of CH₂O molecule over the three considered forms of the [ScPc]^a complexes helped to stabilize these complexes.

In the optimized structure of the [CH₂O/TiPc]^a complexes (Figure 4), the Ti-O bond distances were found as 1.934, 1.914, and 1.844 Å for the [TiPc]⁻¹, [TiPc]⁰, and [TiPc]⁺¹ complexes, respectively. Therefore, it can be inferred that CH₂O was strongly bonded to the Ti atom in the oxidized state when compared to its counterparts. Furthermore, the main change that happened during the CH₂O adsorption over the [TiPc]⁻¹ and [TiPc]⁰ complexes was the projection of the Ti atom out of the molecular plane of these complexes (~0.15 Å).

Figure 4 also displays the optimized structure of the [CH₂O/VPc]^a complexes. Based on these results, the V-O bond distances were 0.003 and 0.032 Å longer in the reduced and neutral states when compared to the oxidized state of the VPc, respectively. Additionally, the V atom remained about 0.12 Å out of the plane of the [CH₂O/VPc]^a complexes.

It is important to mention that other optimized structure parameters, such as the M-N and N-C bond lengths, did not change dramatically after CH₂O adsorption over the studied complexes, due to the interaction of CH₂O with only the metal ion of the MPcs. Moreover, the Pc molecules only had a role as host for the M atom and created an avenue for the charge transfer during adsorption.

The partial charges of the M atom on the CH₂O/MPcs complexes derived from the NBO analysis are tabulated in Table 2, where it can be seen that the adsorption of CH₂O on the MPcs led to a strong charge transfer between the M atom of MPcs, and oxygen atom of the CH₂O molecule. Generally, the positive charges on the M (Sc, Ti, and V) atom of the [CH₂O/MPc] complexes increased by increasing the positive charge on the whole complex. As can be seen in Figure 4, this charge transfer to the FA gas was closely related to variations of the M-O-CH₂ angle, which demonstrated two conformations, i.e.

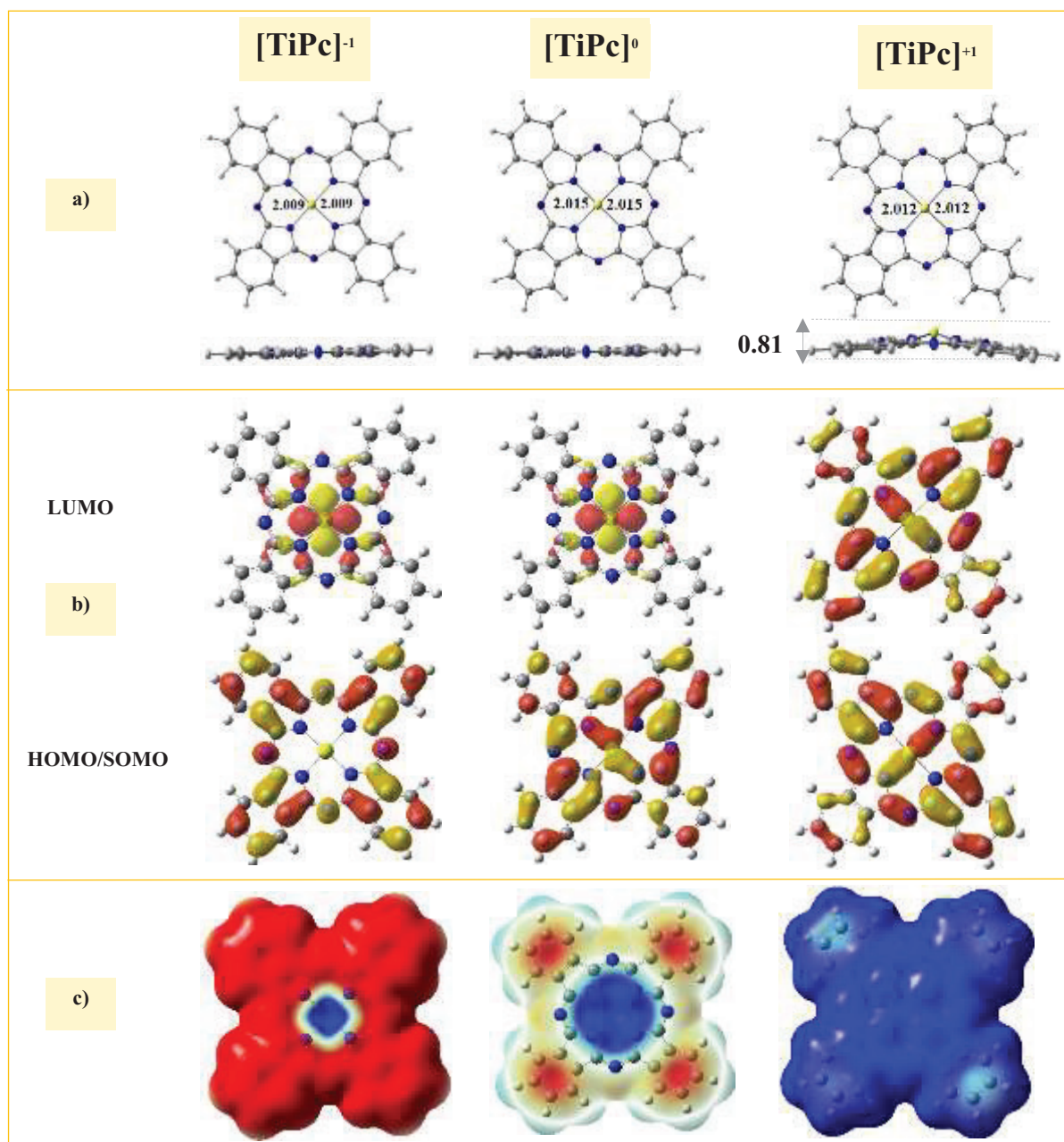


Figure 2. Calculated properties of the $[\text{TiPc}]^a$ ($a = -1, 0, \text{ and } +1$) complexes. a) Top and side views of the optimized structures with the bond distances in Å, b) SOMO/HOMO and LUMO spatial distributions with an isovalue of $0.02 \text{ e}/\text{\AA}^3$, and c) molecular electrostatic potential isosurface (0.0004 au). The C, H, N, and Ti atoms are shown in grey, white, blue, and yellow, respectively.

bent or linear. The concentration of the negative charge in the FA characterized linear geometry ($\angle \text{M-O-CH}_2 = 179.50^\circ$) and was due to the strong interaction between the M atom and CH_2O molecule.

In addition, vibration frequency analysis showed that the vibration mode of C-O bond in the free CH_2O molecule was about 1849 cm^{-1} , while it was significantly red-shifted to $\sim 1261 \text{ cm}^{-1}$ after CH_2O adsorption over the Sc and Ti complexes. It is worth mentioning that the charge was transferred from these molecules to the formally empty π^* orbital of the C-O bond and consequently, weakened this bond. At the same time, π -back bonding occurred from these complexes to the C-O bond. The calculated C-O bond length was about 1.11 and $\sim 1.25 \text{ \AA}$ in the free CH_2O and $[\text{CH}_2\text{O}/\text{MPC}]^a$ ($\text{M} = \text{Sc, Ti, and V}$) complexes, which confirmed the weakening of the C-O bond after adsorption.

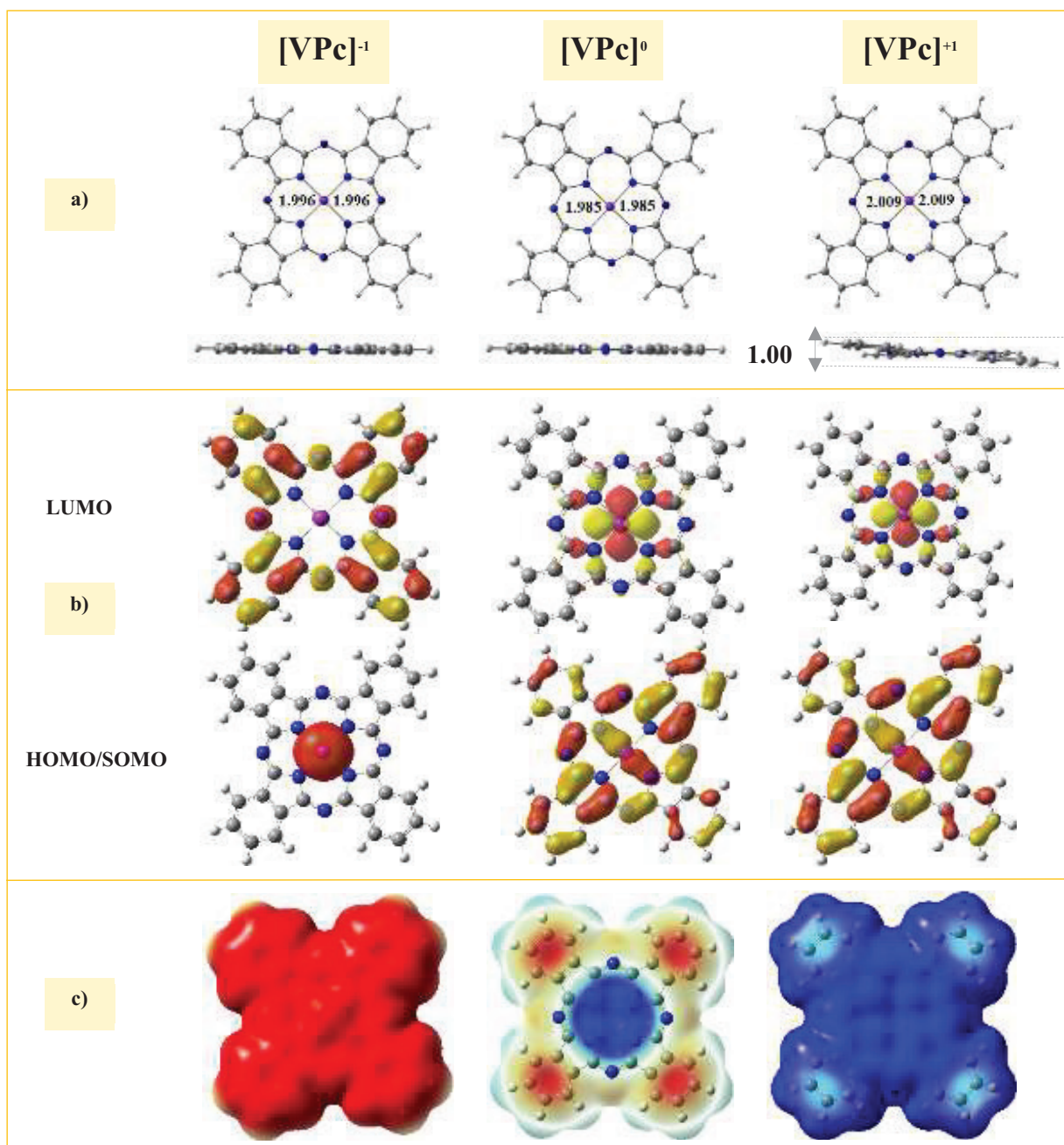
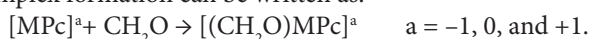


Figure 3. Calculated properties of the $[\text{VPc}]^a$ ($a = -1, 0, \text{ and } +1$) complexes. a) Top and side views of the optimized structures with the bond distances in Å, b) SOMO/HOMO and LUMO spatial distributions with an isovalue of $0.02 \text{ e}/\text{\AA}^3$, and c) molecular electrostatic potential isosurface (0.0004 au). The C, H, N, and V atoms are shown in grey, white, blue, and violet, respectively.

The interaction strength of the $[\text{MPc}]^a$ complexes and CH_2O molecule can be further evaluated by calculating the interacting energy that this interaction led to in the formation of the $[(\text{CH}_2\text{O})\text{MPc}]^a$ complexes. The general reaction of the complex formation can be written as:



The energy values obtained from the calculations of the CH_2O complexation with the $[\text{ScPc}]^{-1}$, $[\text{ScPc}]^0$, and $[\text{ScPc}]^{+1}$ states were -1.51 , -1.55 , and -1.25 eV , respectively (see Table 2). These values showed that the CH_2O molecule was strongly bonded to $[\text{ScPc}]^0$ complex when compared to the $[\text{ScPc}]^{-1}$ and $[\text{ScPc}]^{+1}$ states. As a result of the large negative E_{int} for the $[\text{ScPc}]^a$ complexes, chemical adsorption may occur during CH_2O interaction with the $[\text{ScPc}]^a$ complexes. In the case of

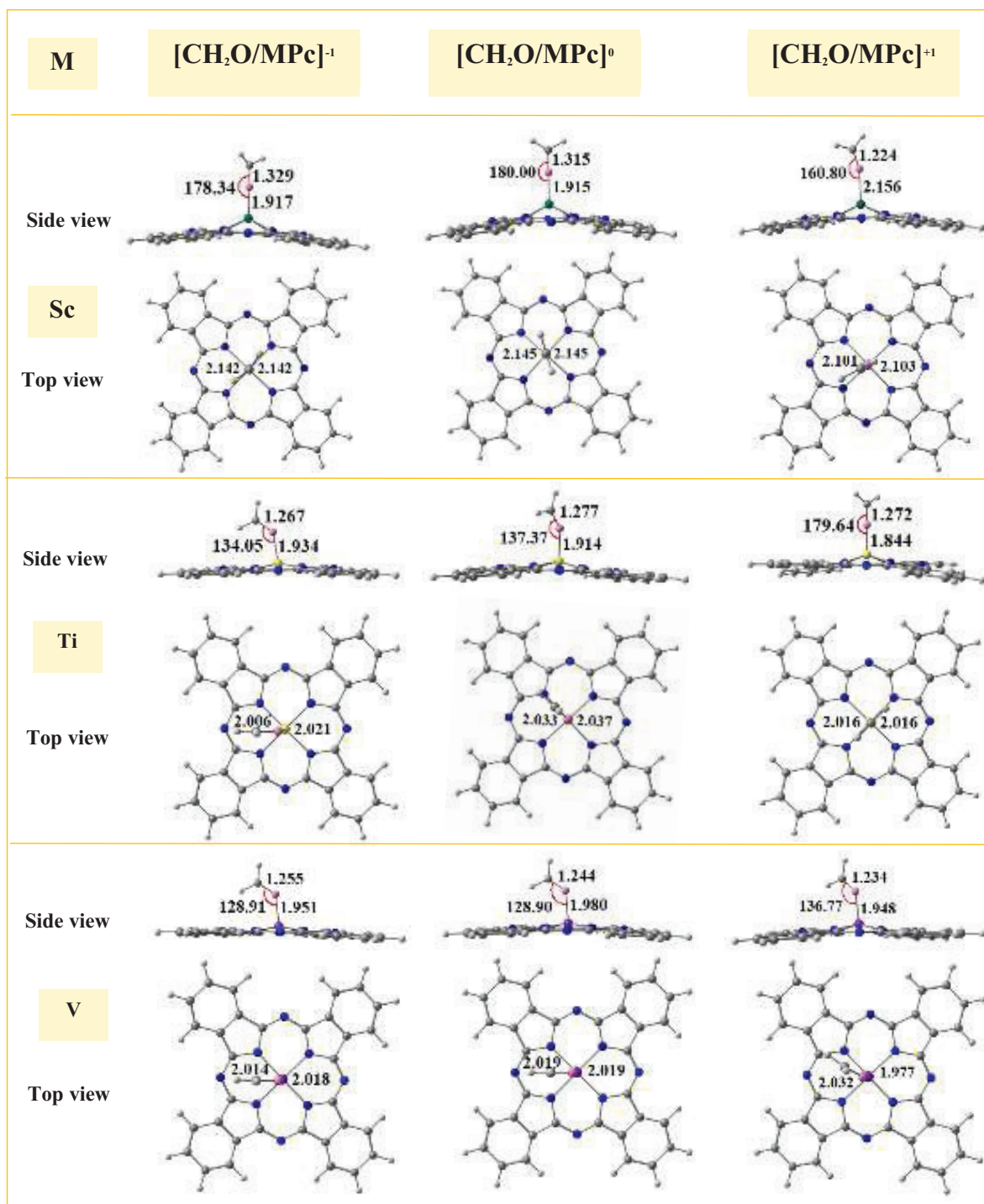


Figure 4. Top and side views of the optimized structures of the $[\text{CH}_2\text{O}/\text{MPc}]^a$ ($M = \text{Sc}, \text{Ti}, \text{and V}, a = -1, 0, \text{and } +1$) complexes with the bond distances in Å and bond angle in degrees. The C, H, N, O, Sc, Ti, and V atoms are shown in grey, white, blue, pink, green, yellow, and violet, respectively.

CH_2O complexation with the $[\text{TiPc}]^{-1}$, $[\text{TiPc}]^0$, and $[\text{TiPc}]^{+1}$ states, the interaction energy values were found as -0.87 , -1.09 , and -1.01 eV, respectively. These results showed that the interaction between CH_2O and the reduced form of the TiPc complexes was weak. The E_{int} values were -0.64 , -2.09 , and -1.06 eV for the $[\text{CH}_2\text{O}/\text{VPc}]^{-1}$, $[\text{CH}_2\text{O}/\text{VPc}]^0$, and $[\text{CH}_2\text{O}/\text{VPc}]^{+1}$ complexes, respectively. As a result, the adsorption of CH_2O on the $[\text{CH}_2\text{O}/\text{VPc}]^{-1}$ complex was weak. These results

Table 2. SOMO¹/HOMO energy ($E_{SOMO/HOMO}$, in eV), LUMO energy (E_{LUMO} , in eV), SOMO/HOMO-LUMO energy gap (E_g , in eV), NBO charge on the M atom in [(CH₂O)MPc] complexes (q_M), NBO charge transfer from [CH₂O/MPc]^a complexes to the CH₂O molecule (Q), and the absolute value of the change in the E_g ($|\Delta E_g|$, %) for the [CH₂O/MPcs]^a (M = Sc, Ti, and V; a = -1, 0, and +1) complexes.

[(CH ₂ O)MPc]	2S + 1	E_g	$E_{SOMO/HOMO}$	E_{LUMO}	E_{int}	q_M	Q	ΔE_g
[CH ₂ O/ScPc] ⁻¹	3	1.06	-0.86	0.20	-1.51	+1.56	-0.24	16
[CH ₂ O/ScPc] ⁰	2	1.15	-4.00	-2.85	-1.55	+1.61	-0.45	2
[CH ₂ O/ScPc] ⁺¹	1	0.95	-7.59*	-6.63	-1.25	+1.69	-0.19	48
[CH ₂ O/TiPc] ⁻¹	2	1.74	-1.10	0.63	-0.87	+1.20	-0.17	21
[CH ₂ O/TiPc] ⁰	1	1.52	-4.32*	-2.80	-1.09	+1.27	-0.15	36
[CH ₂ O/TiPc] ⁺¹	4	1.32	-7.18	-5.86	-1.01	+1.31	-0.23	16
[CH ₂ O/VPc] ⁻¹	3	2.13	-1.68	0.45	-0.64	+0.80	0.02	2
[CH ₂ O/VPc] ⁰	4	2.23	-4.89	-2.66	-2.09	+0.82	0.07	5
[CH ₂ O/VPc] ⁺¹	3	1.26	-7.75	-6.48	-1.06	+0.93	-0.10	6

* Values with asterisks are related to the energy of HOMO.

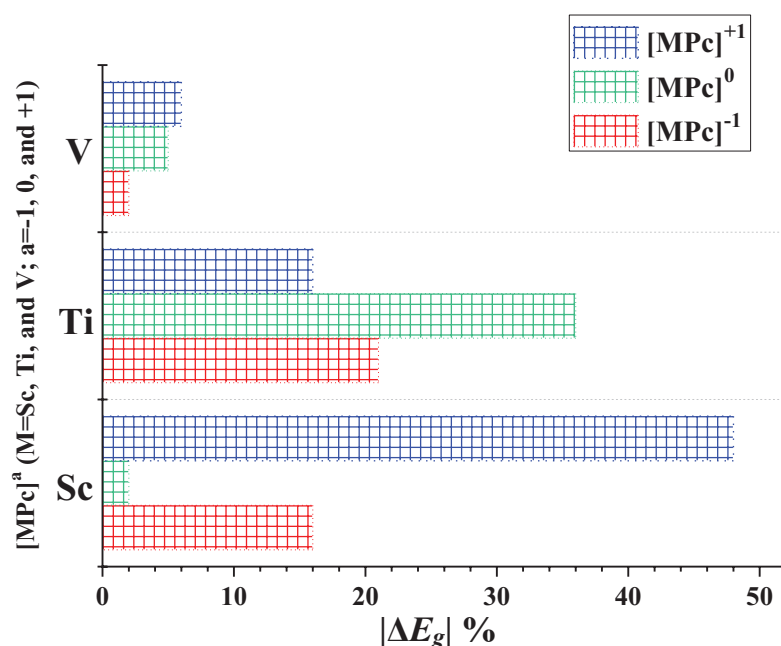


Figure 5. Absolute value of the change in the E_g (ΔE_g) for the [MPcs]^a (M = Sc, Ti, and V, a = -1, 0, and +1) complexes.

were further supported by the negligible charge transfer between CH₂O and the [CH₂O/VPc]⁻¹ complex (see Table 2).

In experimental studies, the variation in electrical conductivity after gas adsorption was measured as a sign of the sensitivity of an electronic sensor toward a specific molecule [45,46]. In theoretical studies, the change of E_g was considered as a characteristic of the sensor to simulate electrical conductivity [47,48]. In this regard, the ScPc and TiPc complexes that showed a decrease in E_g after CH₂O adsorption could demonstrate high electrical conductivity. In other words, by tracing the electrical conductivity variation of the ScPc and TiPc complexes before and after CH₂O adsorption, the presence of this molecule can be detected in the air (see Figure 5). Moreover, among the studied forms of the MPC complexes, it was determined that the [ScPc]⁺¹ and [TiPc]⁰ complexes can be a promising CH₂O sensing material due to the significant decrease in E_g after CH₂O adsorption. This result was confirmed by the total density of the state plots (TDOS) of CH₂O

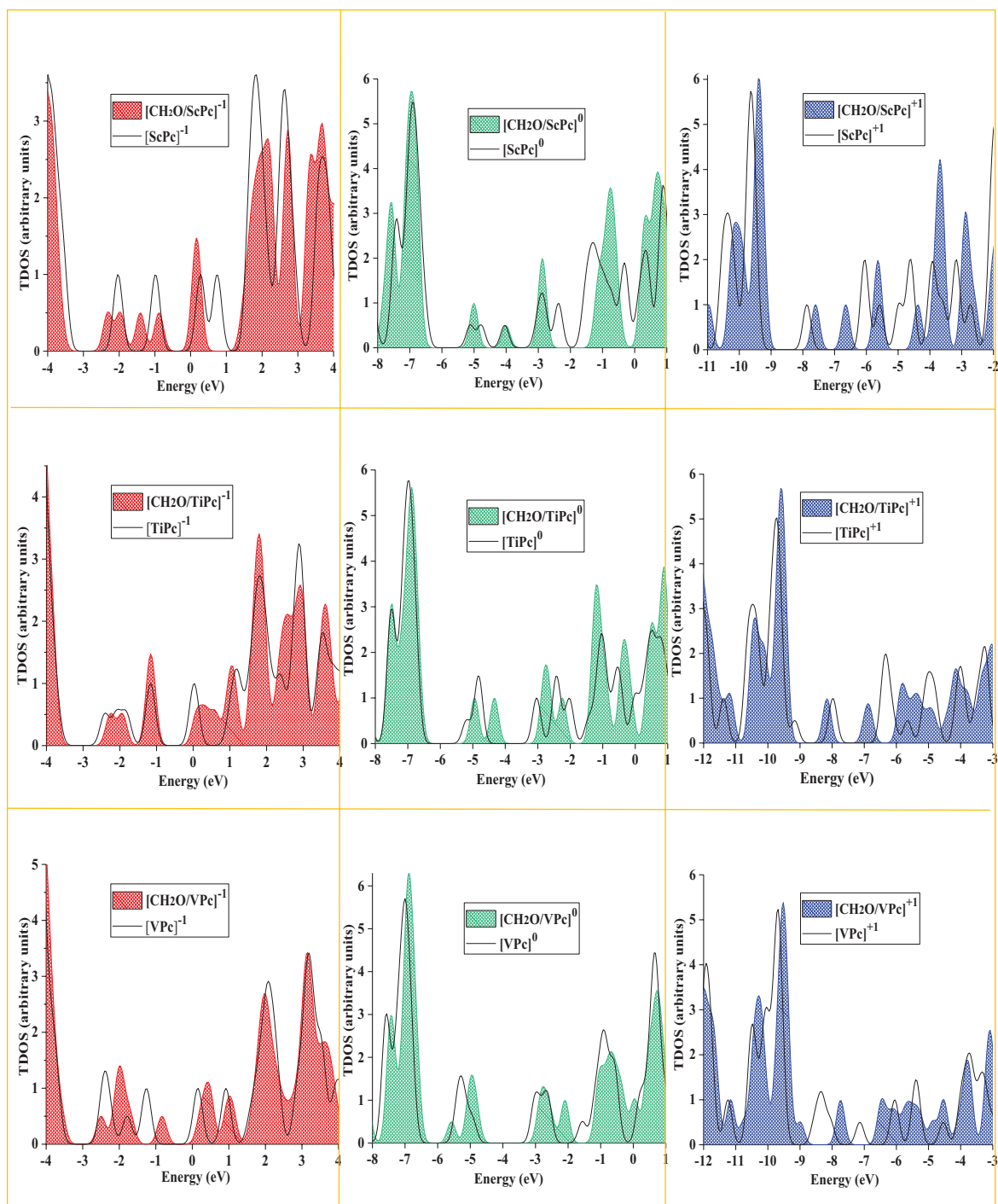


Figure 6. TDOS plots for the $[MPC]^a$ complexes (black curves) and $[CH_2O/MPC]^a$ ($M = Sc, Ti, \text{ and } V, a = -1, 0, \text{ and } +1$) complexes (color-filled curves).

adsorption over the MPC complex (see Figure 6), where the appearance of a new peak between the HOMO and LUMO after adsorption led to a decrease in the E_g value of the $[ScPc]^{+1}$ and $[TiPc]^0$ complexes. In addition to these results, Figure 4a indicated that, in the case of $[ScPc]^0$, the newly formed Sc-O bond in comparison with other M-O bonds in the neutral form of MPCs was short (1.915 Å), but the E_g value (see Table 2) after adsorption changed somewhat (~ 0.03 eV), due to significant structural distortion. Moreover, the adsorption of CH_2O over the vanadium complexes did not alter the E_g

value, due to the distortion of the structure of the VPc complexes after CH₂O adsorption. It is important to mention that, the calculations herein were 298.15 K and 1 atm. However, the calculation results at other temperatures, pressures, and FA concentrations might be different, which should be taken into consideration by experimental and theoretical researchers in future studies.

4. Conclusions

First-principle calculations were performed to study the adsorption and interaction of the CH₂O molecule toward a variety of [MPc]^a (M = Sc, Ti, and V; a = -1, 0, and +1) complexes. It was found that the adsorption of CH₂O over the MPCs was able to significantly alter the electronic properties of the Sc and Ti complexes. The results of the present study revealed that the most pronounced effect on the electronic structure of the MPCs was observed with [ScPc]⁺¹, where the E_g value of [ScPc]⁺¹ showed a variation of about 48% after CH₂O adsorption. It is expected that the present study will stimulate experimental efforts to confirm the results of this work as well as devise chemical modification strategies to design effective MPCs-based gas sensors by employing MPc (M = Sc, Ti, and V) complexes.

Acknowledgement

The author gratefully acknowledges Shiraz University for their generous allocation of computational resources.

References

1. Pestryakov AN. Modification of silver catalysts for oxidation of methanol to formaldehyde. *Catalysis Today* 1996; 28 (3): 239-244. doi: 10.1016/0920-5861(95)00239-1
2. Vohs JM, Barteau MA. Conversion of methanol, formaldehyde and formic acid on the polar faces of zinc oxide. *Surface Science* 1986; 176 (1-2): 91-114. doi: 10.1016/0039-6028(86)90165-2
3. Maroto A, Balasubramanian K, Burghard M, Kern K. Functionalized metallic carbon nanotube devices for pH sensing. *ChemPhysChem* 2007; 8 (2): 220-223. doi: 10.1002/cphc.200600498
4. Liu Z, Searson PC. Single nanoporous gold nanowire sensors. *The Journal of Physical Chemistry B* 2006; 110 (9): 4318-4322. doi: 10.1021/jp056940t
5. Wang J. Biomolecule-functionalized nanowires: from nanosensors to nanocarriers. *ChemPhysChem* 2009; 10 (11): 1748-1755. doi: 10.1002/cphc.200900377
6. Shao MW, Shan YY, Wong NB, Lee ST. Silicon nanowire sensors for bioanalytical applications: glucose and hydrogen peroxide detection. *Advanced Functional Materials* 2005; 15 (9): 1478-1482. doi: 10.1002/adfm.200500080
7. Shao MW, Yao H, Zhang ML, Wong NB, Shan YY et al. Fabrication and application of long strands of silicon nanowires as sensors for bovine serum albumin detection. *Applied Physics Letters* 2005; 87 (18): 183106. doi: 10.1063/1.2123393
8. Liu H, Kameoka J, Czaplewski DA, Craighead HG. Polymeric nanowire chemical sensor. *Nano Letters* 2004; 4 (4): 671-675. doi: 10.1021/nl049826f
9. Shipway AN, Katz E, Willner I. Nanoparticle arrays on surfaces for electronic, optical, and sensor applications. *ChemPhysChem* 2000; 1 (1): 18-52. doi: 10.1002/1439-7641(20000804)1:1<18::AID-CPHC18>3.0.CO;2-L
10. Dovgolevsky E, Konvalina G, Tisch U, Haick H. Monolayer-capped cubic platinum nanoparticles for sensing nonpolar analytes in highly humid atmospheres. *The Journal of Physical Chemistry C* 2010; 114 (33): 14042-14049. doi: 10.1021/jp105810w
11. Tiemann M. Porous metal oxides as gas sensors. *Chemistry—A European Journal* 2007; 13 (30): 8376-8388. doi: 10.1002/chem.200700927
12. Klyamer D, Sukhikh A, Gromilov S, Krasnov P, Basova T. Fluorinated metal phthalocyanines: interplay between fluorination degree, films orientation, and ammonia sensing properties. *Sensors* 2018; 18 (7): 2141. doi: 10.3390/s18072141
13. Mphuthi NG, Adekunle AS, Ebenso EE. Electrocatalytic oxidation of Epinephrine and Norepinephrine at metal oxide doped phthalocyanine/MWCNT composite sensor. *Scientific Reports* 2016; 6: 26938. doi: 10.1038/srep26938
14. Ridhi R, Saini GSS, Tripathi SK. Sensing of volatile organic compounds by copper phthalocyanine thin films. *Materials Research Express* 2017; 4 (2): 025102. doi: 10.1088/2053-1591/aa54d1
15. Peisert H, Schwieger T, Auerhammer JM, Knupfer M, Golden MS et al. Order on disorder: Copper phthalocyanine thin films on technical substrates. *Journal of Applied Physics* 2001; 90 (1): 466-469. doi: 10.1063/1.1375017
16. Jiang H, Ye J, Hu P, Wei F, Du K et al. Fluorination of metal phthalocyanines: Single-crystal growth, efficient n-channel organic field-effect transistors, and structure-property relationships. *Scientific Reports* 2014; 4: 7573. doi: 10.1038/srep07573

17. Abramczyk H, Brozek-Pluska B, Surmacki J, Musial J, Kordek R. Oncologic photodynamic diagnosis and therapy: confocal Raman/fluorescence imaging of metal phthalocyanines in human breast cancer tissue in vitro. *Analyst* 2014; 139 (21): 5547-5559. doi: 10.1039/C4AN00966E
18. Allen CM, Sharman WM, Van Lier JE. Current status of phthalocyanines in the photodynamic therapy of cancer, *Journal of Porphyrins and Phthalocyanines* 2001; 5 (02): 161-169. doi: 10.1002/jpp.324
19. Sizun T, Bouvet M, Chen Y, Suisse JM, Barochi G et al. Differential study of substituted and unsubstituted cobalt phthalocyanines for gas sensor applications. *Sensors and Actuators B: Chemical* 2011; 159 (1): 163-170. doi: 10.1016/j.snb.2011.06.067
20. Bohrer FI, Colesniuc CN, Park J, Ruidiaz ME, Schuller IK et al. Comparative gas sensing in cobalt, nickel, copper, zinc, and metal-free phthalocyanine chemiresistor. *Journal of the American Chemical Society* 2009; 131 (2): 478-485. doi: 10.1021/ja803531r
21. Parkhomenko RG, Sukhikh AS, Klyamer DD, Krasnov PO, Gromilov S et al. Thin films of unsubstituted and fluorinated palladium phthalocyanines: Structure and sensor response toward ammonia and hydrogen. *The Journal of Physical Chemistry C* 2017; 121 (2): 1200-1209. doi: 10.1021/acs.jpcc.6b10817
22. Gülmez AD, Polyakov MS, Volchek VV, Kostakoğlu ST, Esenpinar AA et al. Tetrasubstituted copper phthalocyanines: correlation between liquid crystalline properties, films alignment and sensing properties. *Sensors and Actuators B: Chemical* 2017; 241: 364-375. doi: 10.1016/j.snb.2016.10.073
23. Radhakrishnan S, Deshpande S. Conducting polymers functionalized with phthalocyanine as nitrogen dioxide sensors. *Sensors* 2002; 2 (5) 185-194. doi: 10.3390/s20500185
24. Dong Z, Kong X, Wu Y, Zhang J, Chen Y. High-sensitive room-temperature NO₂ sensor based on a soluble n-type phthalocyanine semiconductor. *Inorganic Chemistry Communications* 2017; 77: 18-22. doi: 10.1016/j.inoche.2017.01.023
25. Aziz F, Sayyad MH, Sulaiman K, Majlis BH, Karimov KS et al. Influence of humidity conditions on the capacitive and resistive response of an Al/VOPc/Pt co-planar humidity sensor. *Measurement Science and Technology* 2001; 23 (11): 014001. doi: 10.1088/0957-0233/23/1/014001
26. Wang WB, Li XG, Wang SR, Hou W. The preparation of high photosensitive TiOPc. *Dyes and Pigments* 2007; 72 (1): 38-41. doi: 10.1016/j.dyepig.2005.07.014
27. Eguchi K, Nakagawa T, Takagi Y, Yokoyama T. Direct synthesis of vanadium phthalocyanine and its electronic and magnetic states in monolayers and multilayers on Ag (111). *The Journal of Physical Chemistry C* 2015; 119 (18): 9805-9815. doi: 10.1021/jp512935v
28. Blowey PJ, Maurer RJ, Rochford LA, Duncan DA, Kang JH et al. The Structure of VOPc on Cu (111): Does V=O Point Up, or Down, or Both?. *The Journal of Physical Chemistry C* 2018; 123 (13): 8101-8111. doi: 10.1021/acs.jpcc.8b07530
29. Lü K, Jian Z, Le Z, Qian W, Qiang S et al. Sc-phthalocyanine sheet: Promising material for hydrogen storage. *Applied Physics Letters* 2011; 99 (16): 163104. doi: 10.1063/1.3653465
30. Arokiyanathan AL, Lakshmipathi S. Impact of functional groups substitution on the molecular properties of magnesium and scandium phthalocyanines. *Inorganica Chimica Acta* 2018; 483: 203-210. doi: 10.1016/j.ica.2018.07.043
31. Becke AD. Density-functional exchange-energy approximation with correct asymptotic behavior. *Physical Review A* 1988; 38 (6): 3098-3100. doi: 10.1103/PhysRevA.38.3098
32. Lee C, Yang W, Parr RG. Development of the Colle-Salvetti correlation-energy formula into a functional of the electron density. *Physical review B* 1988; 37 (2): 785-789. doi: 10.1103/PhysRevB.37.785
33. Frisch MJ, Trucks GW, Schlegel HB, Scuseria GE, Robb MA et al. *Gaussian 09, Revision D.01*, Gaussian, Inc., Wallingford, CT, 2009.
34. Theisen RE, Huang L, Fleetham T, Adams JB, Li J. Ground and excited states of zinc phthalocyanine, zinc tetrabenzoporphyrin, and azaporphyrin analogs using DFT and TDDFT with Franck-Condon analysis. *The Journal of chemical physics* 2015; 142 (9): 094310. doi: 10.1063/1.4913757
35. Jiang H, Ye J, Hu P, Wei F, Du K et al. Fluorination of metal phthalocyanines: Single-crystal growth, efficient n-channel organic field-effect transistors, and structure-property relationships. *Scientific Reports* 2014; 4: 7573. doi: 10.1038/srep07573
36. Chaabene M, Gassoumi B, Mignon P, Chaâbane RB, Allouche AR. New zinc phthalocyanine derivatives for nitrogen dioxide sensors: A theoretical optoelectronic investigation, *Journal of Molecular Graphics and Modelling* 2019; 88: 174-182. doi: 10.1016/j.jmgm.2019.01.008
37. Shalabi AS, Aal SA, Assem MM, Soliman KA. Metallophthalocyanine and Metallophthalocyanine–fullerene complexes as potential dye sensitizers for solar cells DFT and TD-DFT calculations, *Organic Electronics* 2012; 13 (10): 2063-2074. doi: 10.1016/j.orgel.2012.06.028
38. Bakas I, Fourati N, Zerrouki C, Seydou M, Maouche N et al. Surface acoustic wave sensor based on nickel (II) phthalocyanine thin films for organophosphorous pesticides selective detection. *Sensors IEEE* 2014; 321-324. doi: 10.1109/ICSENS.2014.6984998
39. J. Moellmann, S. Grimme, DFT-D3 study of some molecular crystals. *The Journal of Physical Chemistry C* 2014; 118 (14): 7615-7621. doi: 10.1021/jp501237c

40. Boys SF, Bernardi F. The calculation of small molecular interactions by the differences of separate total energies. Some procedures with reduced errors. *Molecular Physics* 1970; 19 (4): 553 -566. doi: 10.1080/00268977000101561
41. Olmsted J, Williams GM. *Chemistry: the Molecular Science*. Jones & Bartlett Learning, 1997.
42. Setvin M, Hulva J, Wang H, Simschitz T, Schmid M et al. Formaldehyde adsorption on the anatase TiO₂ (101) surface: experimental and theoretical investigation. *The Journal of Physical Chemistry C* 2017; 121 (16): 8914-8922. doi: 10.1021/acs.jpcc.7b01434
43. Cortés-Arriagada D, Villegas-Escobar N, Miranda-Rojas S, Toro-Labbé A. Adsorption/desorption process of formaldehyde onto iron doped graphene: a theoretical exploration from density functional theory calculations. *Physical Chemistry Chemical Physics* 2017; 19 (6): 4179-4189. doi: 10.1039/C6CP07710B
44. Abbasi A. Modulation of the electronic properties of pristine and AlP-codoped stanene monolayers by the adsorption of CH₂O and CH₄ molecules: a DFT stud. *Materials Research Express* 2019; 6 (7): 076410. doi: 10.1088/2053-1591/ab1199
45. Choudhuri I, Patra N, Mahata A, Ahuja R, Pathak B. B-N@ Graphene: highly sensitive and selective gas sensor. *The Journal of Physical Chemistry C* 2015; 119 (44): 24827-24836. doi: 10.1021/acs.jpcc.5b07359
46. Huang K, Li Z, Lin J, Han G, Huang P. Two-dimensional transition metal carbides and nitrides (MXenes) for biomedical applications. *Chemical Society Reviews* 2018; 47 (14): 5109-5124. doi: 10.1039/C7CS00838D
47. Faye O, Eduok U, Szpunar JA. Boron-decorated graphitic carbon nitride (g-C₃N₄): an efficient sensor for H₂S, SO₂, and NH₃ capture. *The Journal of Physical Chemistry C* 2019; 123 (49): 29513-29523. doi: 10.1021/acs.jpcc.9b06032
48. Shukla V, Wárná J, Jena NK, Grigoriev A, Ahuja R. Toward the realization of 2D borophene based gas sensor. *The Journal of Physical Chemistry C* 2017; 121 (48): 26869-26876. doi: 10.1021/acs.jpcc.7b09552